



Routes to chaos and bistability in the Rypdal model with a parametric disturbance

Arnold A. Alvarez^{*}, Eduardo L. Brugnago, I.L. Caldas

Instituto de Física, Universidade de São Paulo, São Paulo, SP, Brazil

ARTICLE INFO

Keywords:

Bistability

Shrimp-shaped domains

Attractors reconnection

ABSTRACT

In this work, we propose a parametric perturbation in the plasma production rate of the Rypdal model. This low-dimensional Lorenz-like system is derived from a two-field model for transport in Helimak magnetically confined plasmas. We analyze the stability of the equilibrium points and study the emergence of chaos in the disturbed system. As a perturbation result, the attractor structure is modified, and shrimp-shaped domains occur in the parameter plane, where there are periodic spirals immersed in the chaotic region, both behaviors characterized by the largest Lyapunov exponent. Along these periodic domains, we identify the bistability of attractors, period-doubling cascades, and a route to chaos via bifurcations and collisions of periodic orbits. By the isospikes per period, we schematize the hierarchical organization of periodic attractors into the shrimp spirals.

1. Introduction

Deterministic dynamical systems are widely used as mathematical models in several areas of contemporary science, such as computational neurodynamics [1], epidemiological models [2,3], and confined plasmas [4], either by means of continuous-time or discrete-time approaches. Investigations of nonlinear systems expand the comprehension of the modeled phenomena and the knowledge about chaotic dynamics. Since Lorenz's precursor work [5], a great diversity of autonomous continuous-time nonlinear systems have been studied using computer simulations. These systems, with just three first-order ordinary differential equations, show rich dynamics, such as the Rössler system [6], Rikitake's geomagnetic model [7], and Chua's circuit [8], to name a few paradigmatic ones. Nowadays, variations of these models including parametric perturbations have been proposed [9,10].

The parametric configuration plays a determining role in the evolution of nonlinear dynamical systems. Understand the parameters influence on the transitions between periodic and chaotic behavior is indispensable to deepen the knowledge of these models, with applications to countless phenomena. As tools to characterize solutions of a given system, it is usual to analyze the Lyapunov spectrum [11,12], the period [13–15], or the number of isospikes [16,17]. These quantities are typically represented in plane sections of parameter space if there are two or more parameters, thus providing an optimal and simple visualization of the dynamic behavior due to the parameter values. In the numerical approach, Lyapunov exponents are broadly used, as they allow an easy distinction between periodic or quasiperiodic behavior

from chaotic dynamics. For a more detailed characterization of the dynamics in continuous-time systems, the Lyapunov spectrum and the isospike count can be analyzed together.

It is known that both continuous and discrete-time systems can exhibit periodic regions in the form of shrimps immersed in chaotic areas of the parameter plane [12,15,16,18,19]. Perhaps more fascinating, these shrimp-shaped domains can be organized into spiral structures [18,20–22], a phenomenon that has a close relationship with the existence of homoclinic connections [23,24] involving saddle-foci that satisfies the single Shilnikov criterion [18,25]. Barrio et al. [18] demonstrate that a line passing through the superstable crosses, into the spiral shrimp-shaped domains, delimits a topological change in the chaotic attractors structure.

Periodic parametric perturbations in the diffusionless Lorenz equations, presenting similarities with the Rypdal model, as a chaos control mechanism was extensively studied by Yang and Wei [26,27]. In this work, we propose an exponential parametric disturbance on the Rypdal model [28,29], resulting in a new unstable equilibrium point, causing a significant enrichment of the dynamics and maintaining the symmetry properties of the original system.

As primary motivation, we investigate the dynamics into the shrimp-shaped domains constituting the spiral structure observed in a parameter plane of the disturbed model. We analyze the Lyapunov exponents together with counting local maxima per period (isospikes) and determine the coexistence regions of the periodic attractors in

^{*} Corresponding author.

E-mail address: arnold@if.usp.br (A.A. Alvarez).

symmetric-pairs [30]. Additionally, to draw a general idea of the process that leads to the chaos emergence in the disturbed model, we obtain and study bifurcation diagrams along curves in the parameter plane as well as show a schematic diagram of these routes to chaos.

This article is organized as follows: Section 2 deal with the original Rypdal model. We determine the equilibrium points stability and analyze Lyapunov spectra together an isospikes count along the parameter plane. In Section 3, we propose a parametric disturbance to the Rypdal model and obtain the fixed points stability, as well as investigate the disturbed system dynamics. We talk about the two distinct routes to chaos in the parameter plane and bistability domains. Section 4 summarizes our main results.

2. Rypdal model

The Rypdal model has been proposed to describe the behavior of magnetically confined plasmas in Helimaks [28]. It consists of a bi-parametric system of three ordinary differential equations given by

$$\begin{aligned}\dot{x} &= -\nu x - y, \\ \dot{y} &= x(1 - z), \\ \dot{z} &= xy + s,\end{aligned}\quad (1)$$

where x and y are the potential and perturbed electron density amplitudes, respectively, and the variable z quantifies the strength of the pressure profile gradient that drives instability. It is related with the anomalous flux due to the convection cells. This model is symmetric under the transformation

$$T : (x, y, z) \mapsto (-x, -y, z), \quad (2)$$

i.e., the equations system are invariant under a π -rotation around the z -axis [31]. The parameter ν represents the momentum loss resulting from collisions between ions and neutral particles, whereas s is the effective plasma production rate. In this study, we consider $s > 0$. Since $\nu > 0$, the system (1) is dissipative: given the flow $\phi = (x, y, z)$, it is verified that $\nabla \cdot \phi = -\nu < 0$.

2.1. Fixed points analysis

From the equilibrium condition $\dot{x} = \dot{y} = \dot{z} = 0$ applied to the system (1), only two fixed points are found:

$$N_{\pm} (x_{\pm}^*, y_{\pm}^*, z^*) = N_{\pm} \left(\pm\sqrt{\frac{s}{\nu}}, \mp\sqrt{sv}, 1 \right). \quad (3)$$

We evaluate the linear stability of these equilibria. It is determined by the eigenvalues of the system's Jacobian matrix \mathbb{J} , calculated at N_{\pm} . We get

$$\mathbb{J}|_{N_{\pm}} = \begin{bmatrix} -\nu & -1 & 0 \\ 0 & 0 & \mp\sqrt{s/\nu} \\ \mp\sqrt{sv} & \pm\sqrt{s/\nu} & 0 \end{bmatrix}, \quad (4)$$

whose characteristic polynomial is independent of the specific fixed point, due to the symmetry (2), as follows:

$$P(\xi) = \xi^3 + \nu\xi^2 + \frac{s}{\nu}\xi + 2s. \quad (5)$$

Since $s, \nu > 0$, result one real eigenvalue $\xi_1 < 0$ and the others $\xi_{2,3}$ as a complex conjugate pair with positive real part. Thus, relative to N_{\pm} there is a one-dimensional stable and a two-dimensional unstable invariant manifolds. Therefore, both equilibrium points are unstable, being saddle-foci of (1,2)-type [20].

Given an initial condition $C_0(x_0, y_0, z_0)$ in the systems phase space, the trajectory converges to an attractive orbit evolving in turns around the unstable equilibria N_{\pm} . Fig. 1 shows four attractors obtained from $C_0(0.01, 0.01, 1)$ for different parametric configurations. To reach them, we numerically integrate the system (1) using the Fehlberg Runge-Kutta 5(6) method [32] with a time step of 10^{-3} . The first 5×10^7

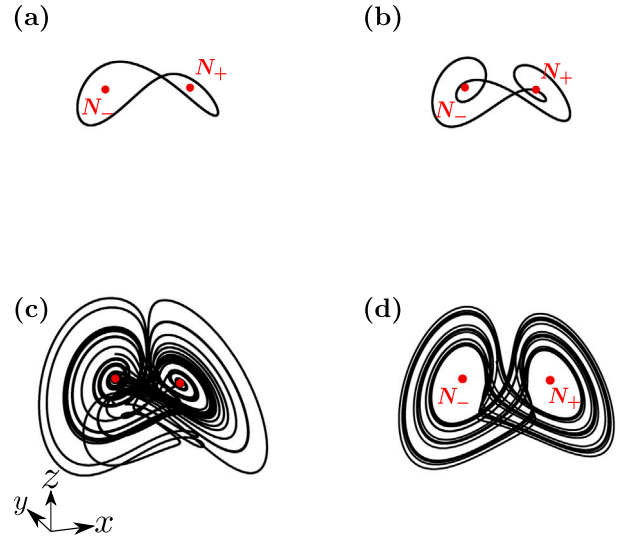


Fig. 1. Rypdal model attractors around the unstable equilibria N_{\pm} (red points). Used the same initial condition $C_0(0.01, 0.01, 1)$ and the parameter $s = 1$ in all panels. Discarded a transient of 5×10^7 integration steps. Periodic attractors of: (a) period-1 for $\nu = 0.4678$; (b) period-3 for $\nu = 0.7443$. Chaotic attractors of: (c) Sprott B typical shape for $\nu = 0.9812$; (d) Burke-Shaw type [31,35] chaotic one. Just like the Sprott B system, the Rypdal model does not present Lorenz-like attractors [34, 35].

iterations were discarded as transient and the subsequent 5×10^5 trajectory points were used. In Figs. 1(a) and (b) we present two periodic orbits. Regarding the similarity between system (1) and Sprott B [33,34], evidenced by the transformations discussed in Section 2.2.1, in Fig. 1(c) we show a typical Sprott B chaotic attractor. While Fig. 1(d) displays a Burke-Shaw type [31,35] chaotic one. Just like the Sprott B system, the Rypdal model does not present Lorenz-like attractors [34, 35].

2.2. Parameter plane $s \times \nu$

The parameters influence on the Rypdal model dynamics is evidenced by the Lyapunov exponents and isospikes diagram [16], both computed along the $s \times \nu$ parameter plane shown in the top panels Fig. 2. In each of the three, a color code represents the different measurements taken. We evaluate the parameter ranges $s \in (0, 10]$ and $\nu \in (0, 3.2]$ discretized in a uniform grid of 1000×1000 points. The Lyapunov spectrum was determined using the algorithm described by Wolf et al. [36,37], with the exponents ordered $\lambda_1 \geq \lambda_2 > \lambda_3$. Isospikes were counted as the number p of local maxima in the x variable series during a full lap in periodic solutions, which is referred to as I_p along this paper.

There is a technical consideration on the Lyapunov spectrum computation, for which the Fehlberg method, or another similar low-cost integration scheme, did not provide convergence, resulting in spurious fluctuations. Considering this fact, to evolve the system (1), we implement two numerical integration stages. First, we adopt the Fehlberg Runge-Kutta 5(6) method with a constant time step of 10^{-2} and discard as transient 10^5 iterations. This stage reduces the computational cost for orbit convergence. In sequence, we continue the integration with the Prince-Dormand Runge-Kutta 8(7) method [38], maintaining the time step and with a transient of 2×10^6 iterations. The Lyapunov spectrum was computed over the subsequent 2×10^6 iterations. We take as initial condition $C_0(0.01, 0.01, 1)$.

Fig. 2(a.1) shows the largest Lyapunov exponent when $\lambda_1 > 0$ (signature of chaotic dynamics) in shades from red to yellow. While in periodic cases ($\lambda_1 = 0$), the second exponent $\lambda_2 \leq 0$ is shown in shades from cyan to black. The central chaotic band is bordered by a

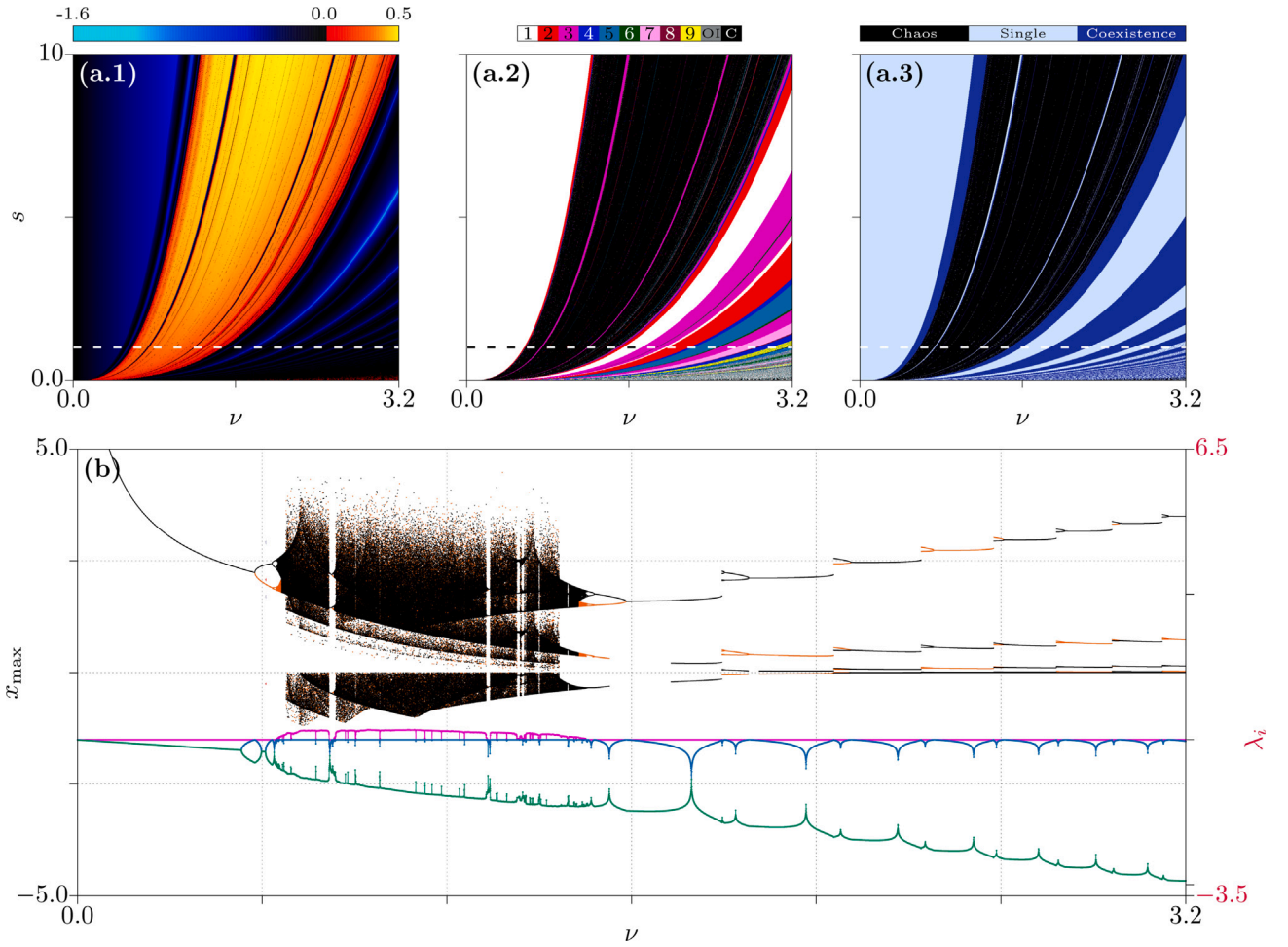


Fig. 2. Top panels show the parameter plane $s \times \nu$ discretized in a uniform grid of 1000×1000 points. Three different measurements are color-coded, being: (a.1) largest Lyapunov exponent $\lambda_1 > 0$ for chaotic solutions (gradient from red to yellow) and $\lambda_2 \leq 0$ (from cyan to black) in the periodic cases; (a.2) isospikes in x variable for periodic attractors, chaotic bands are in black color, and isospike values besides the numeric legend are in gray color; (a.3) periodic attractors coexistence in dark blue and single solution in light blue color. (b) Bifurcation diagram and Lyapunov spectrum along the dashed line $s = 1$ (present in the upper panels). Local maxima of x for attractors obtained from the initial condition $C_0(0.01, 0.01, 1)$ (black dots) and $C'_0(-0.01, -0.01, 1)$ (orange dots). Exponents: λ_1 (magenta line), λ_2 (blue line) and λ_3 (green line). (For interpretation of the references to color in this figure legend, the reader is referred to the web version of this article.)

cubic relationship between the parameters s and ν , a fact discussed at the end of this section (see Section 2.2.1). There are narrow periodic windows throughout this wide chaotic range. Fig. 2(a.2) display the isospikes counting, chaos is represented in black color (C), and isospike values besides the numeric legend are in gray color (OI). On the right of this figure, there is a bifurcation from I_1 (white color) to I_2 (red color) and, on the other side of the white stripe, a isospike change from I_1 to I_3 (magenta). Following a vertical line from $s = 0$ to $s = 10$, a sequence of different isospike values is observed in $\nu = 3.2$.

Another characteristic of the Rypdal model, due to the system's symmetry transformation (2), is the occurrence of bistability for certain parametric configurations, where the system exhibits a symmetric-pair of attractive solutions [31,39]. In these cases, two distinct attractors $\mathcal{A} \neq \mathcal{A}'$ coexist, such that the symmetry transformation (2) leads $T(\mathcal{A}) = \mathcal{A}'$ and $T(\mathcal{A}') = \mathcal{A}$. Fig. 2(a.3) distinguishes regions with only one periodic attractor (light blue) from those with bistability (dark blue). Regarding the attraction basin \mathcal{B} of \mathcal{A} (and \mathcal{B}' of \mathcal{A}'), there is $T(\mathcal{B}) = \mathcal{B}'$ and vice-versa.

Fig. 2(b) presents a bifurcation diagram and the Lyapunov spectrum along the horizontal dashed line $s = 1$, marked in (a.1–3) panels. We consider the local maxima (x_{\max}) of x variable time series and evolve the system from the initial conditions C_0 (black dots) and $T(C_0)$ (orange dots). In this way, bistable ν intervals can be identified. The Lyapunov spectrum coincides for \mathcal{A} and \mathcal{A}' , being the magenta line for λ_1 , blue

for λ_2 and green for λ_3 . For ν values close to zero, the bifurcation diagram shows a periodic orbit with just one spike per period (I_1 attractor). Subsequently, with $\nu \approx 0.52$, a pitchfork bifurcation takes to the coexistence of two I_1 symmetric attractors. Following this, a period-doubling bifurcations cascade occurs, leading to a chaotic range. With $\nu \approx 0.6$, a sudden expansion of the chaotic attractor is due to an internal crisis [40]. Along the chaotic region, the system exhibits an infinite number of periodicity windows, some of which show bistability. For values higher than $\nu \approx 1.475$, it is observed a crises sequence involving period-doubling bifurcations and isospikes increment rule in which the periodic symmetric-pair merges into one single attractor.

2.2.1. Rescaling variables

Before rescaling the system (1), we consider the linear substitution of z to $(z - 1)$. The scale transformation involves the parameter s and also applies to time [39], being:

$$R_s : (x, y, z, t) \mapsto (s^{1/3}x, s^{2/3}y, s^{2/3}z, s^{-1/3}t). \quad (6)$$

Thus, the following system is obtained:

$$\begin{aligned} \dot{x} &= -\nu'x - y, \\ \dot{y} &= -xz, \\ \dot{z} &= xy + 1, \end{aligned} \quad (7)$$

with only one control parameter $\nu' = \nu s^{-1/3}$.

This transformation does not change the system form. All attractors along the curve $s = Cv^3$, with C being a constant, exhibit the same behavior in terms of stability and isospikes. This result explains the curves observed in the plane $s \times v$ shown in Figs. 2(a.1–3). The similarity between Eqs. (7) and the Sprott B system is notable [33]. Under the appropriate linear transformations [34], a Sprott B is obtained from the Rypdal model, for example, replacing x to $-x$ in Eqs. (7).

3. Modified rypdal model

In this section, we propose a parametric exponential disturbance in the third equation of the Rypdal model. This perturbation acts as a control on plasma generation and can be interpreted as the presence of a channel that leads to a reduction in the plasma production rate. Such control is proportional to the pressure profile gradient.

The proposal consists of replacing the solitary parameter s according to:

$$s \mapsto s(1 - \epsilon e^{\gamma z}), \tag{8}$$

where an exponential response occurs depending on the variable z . Being $0 < \gamma$ and $0 < \epsilon \ll 1$. Such modification to the system (1), with the previous replacement of z to $(z - 1)$, leads to

$$\begin{aligned} \dot{x} &= -vx - y, \\ \dot{y} &= -xz, \\ \dot{z} &= xy + s(1 - \epsilon e^{\gamma z}), \end{aligned} \tag{9}$$

Just like the original model, the above system is dissipative: the flow divergence is $\nabla \cdot \phi = -(v + s\epsilon\gamma e^{\gamma z}) < 0$. It is worth noting that the symmetry under the transformation (2) is maintained.

3.1. Fixed points analysis

The equilibrium condition applied to the exponentially disturbed Rypdal model (9) gives us three fixed points:

$$O \left(0, 0, -\frac{1}{\gamma} \ln \epsilon \right) \text{ and } N_{\pm} \left(\pm \sqrt{\frac{s'}{v}}, \mp \sqrt{s'v}, 0 \right).$$

The N_{\pm} equilibria are the same form as those obtained for the original model, with $s' = s(1 - \epsilon)$, see Eq. (3). A new feature is the third point O , which exists only in the disturbed model. This new fixed point affects the system dynamics, a subject discussed throughout this section.

To analyze the stability of the equilibrium points found, we proceed by determining the eigenvalues of the system (9) Jacobian matrix evaluated at each one. For the point O , we get:

$$\mathbb{J}|_O = \begin{bmatrix} -v & -1 & 0 \\ \frac{1}{\gamma} \ln \epsilon & 0 & 0 \\ 0 & 0 & -s\gamma \end{bmatrix}, \tag{10}$$

whose characteristic polynomial is

$$P(\zeta) = \left(\zeta^2 + v\zeta + \frac{1}{\gamma} \ln \epsilon \right) (\zeta + s\gamma). \tag{11}$$

From which we obtain the eigenvalues

$$\zeta_1 = -s\gamma; \quad \zeta_{2,3} = -\frac{v}{2} \mp \frac{1}{2} \sqrt{v^2 - \frac{4}{\gamma} \ln \epsilon}.$$

There is $\zeta_{1,2} < 0$ and, since $\epsilon < 1$, $\zeta_3 > 0$. Therefore, the point O is a (2,1)-type saddle point, i.e., with a 2D stable (W_O^s) and 1D unstable (W_O^u) invariant manifolds.

For the other two points, the Jacobian matrix becomes

$$\mathbb{J}|_{N_{\pm}} = \begin{bmatrix} -v & -1 & 0 \\ 0 & 0 & \mp \sqrt{s'/v} \\ \mp \sqrt{s'v} & \pm \sqrt{s'/v} & s\epsilon\gamma \end{bmatrix}. \tag{12}$$

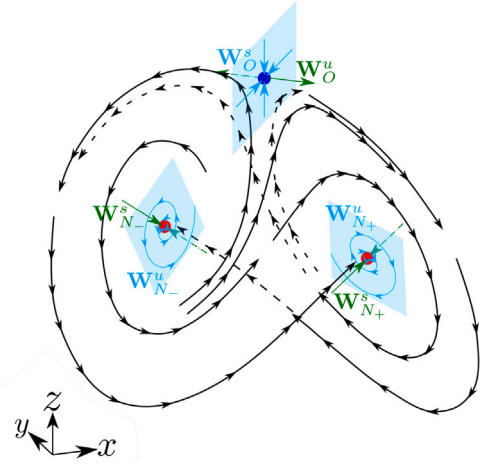


Fig. 3. Scheme of the trajectory evolution around the saddle-foci N_{\pm} (red dots), with incursions close to the saddle point O (blue dot). Local representations of the stable ($W_{N_{\pm}}^s$ and W_O^s) and unstable ($W_{N_{\pm}}^u$ and W_O^u) invariant manifolds. For simplicity, we present a flat portrait of the unstable manifolds of both N_{\pm} . (For interpretation of the references to color in this figure legend, the reader is referred to the web version of this article.)

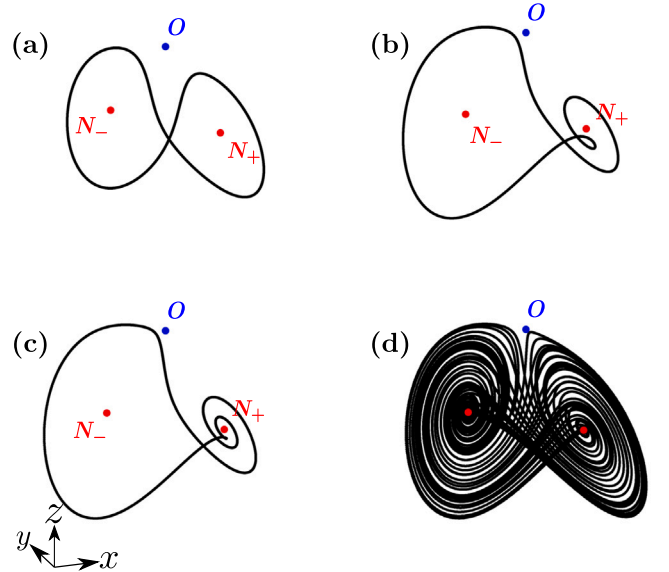


Fig. 4. Disturbed Rypdal model attractors around the unstable equilibria N_{\pm} (red points). Saddle point O highlighted in blue. For all panels was used the initial condition $C_0(0.01, 0.01, 0.01)$, with the parameters $s = 1$ and $\epsilon = 0.01$. Discarded a transient of 5×10^6 integration steps. Periodic attractors with isospikes count p equals to: (a) 1 for $(v, \gamma) = (1.2441, 2.5881)$; (b) 2 for $(v, \gamma) = (0.8250, 2.1811)$; and (c) 3 for $(v, \gamma) = (0.9140, 2.1421)$. (d) Chaotic Lorenz-like attractor for $(v, \gamma) = (0.9818, 2.1115)$. (For interpretation of the references to color in this figure legend, the reader is referred to the web version of this article.)

We have the same characteristic polynomial for both N_{\pm} , as seen for the unperturbed model in Section 2.1, there is

$$P(\xi) = \xi^3 + (s\epsilon\gamma + v)\xi^2 + \left(s\epsilon\gamma v + \frac{s'}{v} \right) \xi + 2s'. \tag{13}$$

Note that these polynomial coefficients are almost the same form as those in Eq. (5). The distinction only due to the term $s\epsilon\gamma$, arising from the exponential perturbation in the z variable. Given the parameter ranges, there is always a real eigenvalue $\xi_1 < 0$. The other two can be real $\xi_{2,3} < 0$ or a complex conjugate pair. By means of the

Routh–Hurwitz criterion [41], we conclude that $\Re(\xi_{2,3}) < 0$ iff

$$\gamma > \frac{\sqrt{(v^3 + s')^2 + 4s'v^3} - (v^3 + s')}{2s\varepsilon v^2}, \quad (14)$$

where the equilibrium points N_{\pm} are stable.

A supercritical Andronov–Hopf (AH) bifurcation [42] occurs by cross the hypersurface

$$\sigma : v^2(s\varepsilon\gamma)^2 + (v^3 + s')s\varepsilon\gamma - s'v = 0, \quad (15)$$

in the parameter space. If the relation (14) is not fulfilled, then the eigenvalues $\xi_{2,3}$ are complex conjugates with real part greater than zero. Exception for the equality between γ and the second member expression that gives the AH. Consequently, N_{\pm} are saddle-foci of (1,2)-type, with a 1D stable ($W_{N_{\pm}}^s$) and 2D unstable ($W_{N_{\pm}}^u$) invariant manifolds, as in the unperturbed model. In such parametric configurations, the trajectories evolve around the equilibria N_{\pm} , being influenced by the manifolds of the saddle point O .

The trajectory stretches in Fig. 3 illustrate how the system evolution occurs. We observe the spiral expansion around one of the saddle-foci (whether N_- or N_+), moving on to orbit the other saddle-focus. Eventually, the trajectory passes close to the O saddle point and is greatly influenced by its manifolds. In this circumstance, is carried upward in the proximity of the stable manifold W_O^s and redirected

towards the spiral when approaching the unstable manifold W_O^u . Fig. 4 shows one chaotic and three periodic attractors. All four were obtained from the same initial condition C_0 and different parameter values. The system evolution can lead to the proximity of N_- or N_+ , as in panels (c) and (d). In the latter, the approach to the saddle point is also observed. The periodic attractors are identified by the isospikes in the variable x : (a) I_1 , (b) I_2 and (c) I_3 . Due to the additional saddle point, the model with perturbation now presents Lorenz-like chaotic attractors [34], as shown in Fig. 4(d). The dynamics of the disturbed Ryrdal model is similar to that of the Lorenz system as it is governed by the equilibrium points manifolds, which are in the same configuration in both systems.

3.2. Parameter plane $\gamma \times v$

System (9) is rescalable by R_s , according to transformation (6), maintaining the equation's form and with the parameter $\gamma' = s^{\frac{2}{3}}\gamma$. In terms of dynamics, this is equivalent to assuming $s = 1$. Given an ε value and a parameter v interval, by means of the relation (14), we find a range of γ that corresponds to stables N_{\pm} . Nevertheless, we aim to investigate the system behavior outside the parametric configurations that lead to stable fixed points, i.e., beyond the border obtained by (14). In particular, we use $\varepsilon = 0.01$. Thus, we focus the study on a region where $\Re(\xi_{2,3}) > 0$ in the plane $\gamma \times v$. Similarly to the

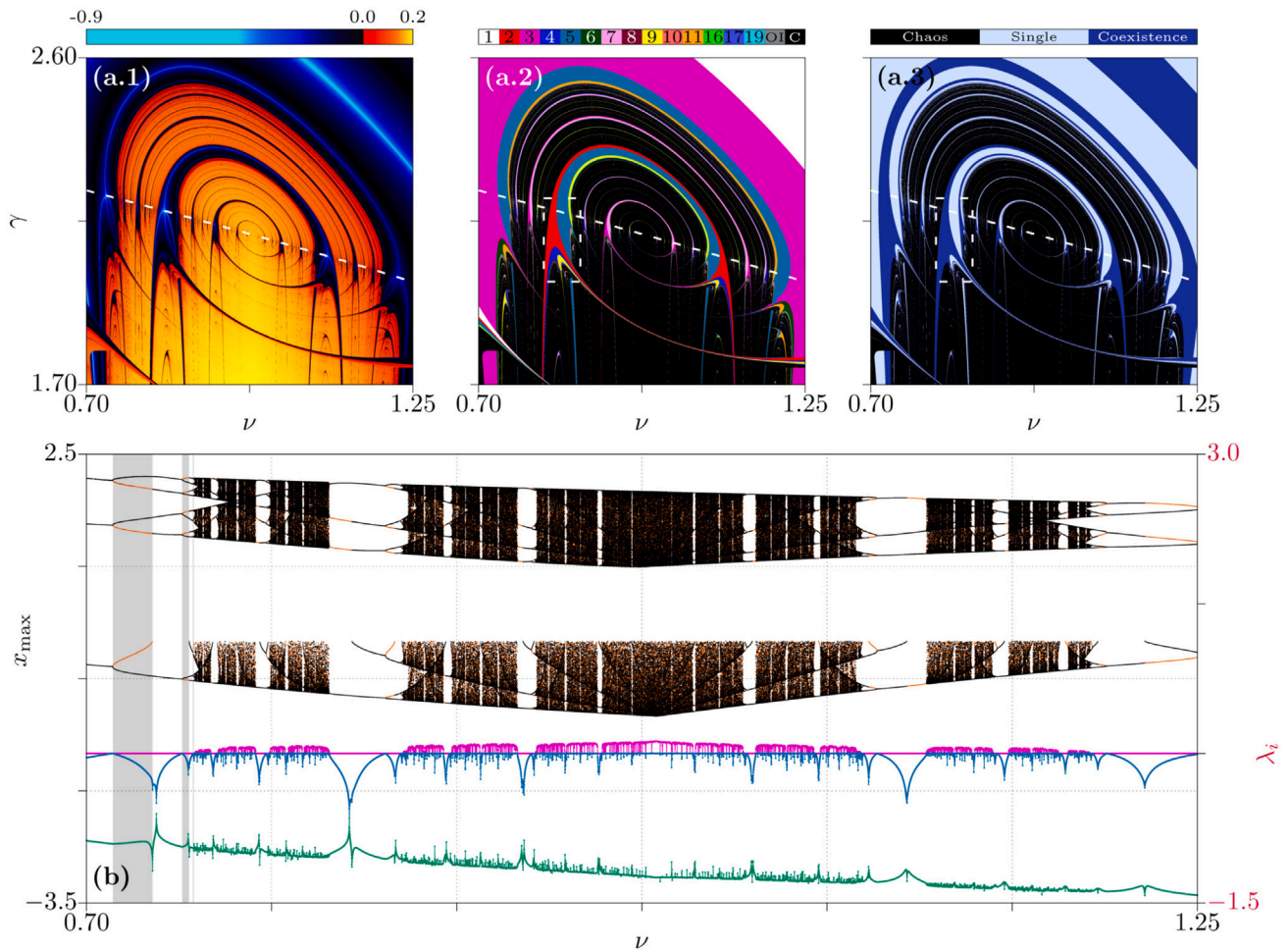


Fig. 5. Top panels show the parameter plane $\gamma \times v$ discretized in a uniform grid of 1000×1000 points. Three different measurements are color-coded, being: (a.1) largest Lyapunov exponent $\lambda_1 > 0$ for chaotic solutions (gradient from red to yellow) and $\lambda_2 \leq 0$ (from cyan to black) in the periodic cases; (a.2) isospikes in x variable for periodic attractors, chaotic bands are in black color, and isospike values besides the numeric legend are in gray color; (a.3) periodic attractors coexistence in dark blue and single solution in light blue color. The highlighted box is magnified in Fig. 7. (b) Bifurcation diagram and Lyapunov spectrum along the dashed curve present in the upper panels. The curve $\gamma(v)$ passes through the superstable points inside the shrimps and is given by Eq. (16). Local maxima of x for attractors obtained from the initial condition $C_0(0.01, 0.01, 0.01)$ (black dots) and $C'_0(-0.01, -0.01, 0.01)$ (orange dots). Exponents: λ_1 (magenta line), λ_2 (blue line) and λ_3 (green line). (For interpretation of the references to color in this figure legend, the reader is referred to the web version of this article.)

analysis performed for the undisturbed model in Section 2.2, here we evaluate the Lyapunov spectrum and isospikes counting.

To numerically evolve the system (9), was used the Fehlberg Runge–Kutta 5(6) method with a constant time step of 10^{-2} . We consider a transient 5×10^6 iterations and compute the spectrum over the subsequent 2×10^6 iterations. The initial condition $C_0(0.01, 0.01, 0.01)$ was adopted. For the exponentially disturbed Rypdal model, the Lyapunov exponents converge faster than for the undisturbed system without the need for an intermediate greater precision numerical integration stage. We also verify the occurrence of symmetric periodic attractor-pair coexistence.

Fig. 5 top panels show the parameter plane $\gamma \times \nu$ discretized in a 1000×1000 uniform grid, being the intervals $\gamma \in (1.7, 2.6]$ and $\nu \in (0.7, 1.25]$. We evaluate three different measurements (in colors): (a.1) Lyapunov exponents (λ_1 and λ_2); (a.2) isospikes in the x variable time series; and (a.3) coexistence of periodic attractors forming a symmetric-pair. Fig. 5(a.1) shows spirals of connected shrimps immersed in the chaotic region ($\lambda_1 > 0$ from red to yellow color). These periodic structures ($\lambda_1 = 0$ and $\lambda_2 < 0$ from cyan to black color) appear in an infinite number of spiral families, with a focal point in a central Hub [30]. Such formations are typical of systems exhibiting homoclinic connections in saddle-focus, fulfilling the Shilnikov condition [18,20].

Into the shrimp-shaped regions shown in Fig. 5(a.2), attractors with different isospikes counting occur apart of the well-known period-doubling bifurcation cascade [43]. For example, the change of I_3 (magenta) to I_5 (teal) in the periodic band surrounding the chaotic area and from I_2 (red) to I_5 in the next big shrimp. These transitions are related to the coexistence of two attractors forming a symmetric-pair, a subject covered in Section 3.2.1. Connected shrimps form pairs with same the I_p strips. Each pair connects to the next one spiraling towards the focal point, adding just one unit to the start-band isospikes count. We refer to the start-band, the lowest I_p strip within a periodic structure, as I_2 (red strip) in the first shrimp pair and I_3 (magenta strip) in the next pair entering the spiral. In Fig. 5(a.3), we identify periodic regions with single attractors (light-blue color) and the bistability with symmetric-pair solutions (dark-blue color). Along the period-doubling bifurcation cascade, two different attractors, \mathcal{A} and \mathcal{A}' , coexist, with the symmetry $T(\mathcal{A}) = \mathcal{A}'$. Following the other observed isospikes sequence, the bands of single and symmetric-solutions are interspersed (see Fig. 9).

The dashed line marked in Figs. 5(a.1–3) corresponds to the cubic polynomial

$$\gamma(\nu) = 2.53519 - 0.465368\nu + 0.0927489\nu^2 - 0.0592718\nu^3, \quad (16)$$

which was adjusted to pass through the high stable crosses in shrimp domains, i.e., through the crossing points of two local minima curves of the second Lyapunov exponent. In the shrimp spiral, the period-doubling bifurcation cascades occur only below the $\gamma(\nu)$ curve. The diagram in Fig. 5(b) shows the dynamic changes along $\gamma(\nu)$, with $\nu \in (0.7, 1.25]$. There are intervals with symmetric-pairs of attractors, where the local x_{\max} of orbits from the initial condition C_0 (black dots) are distinguished from those of $T(C_0)$ (orange dots). Such regions are delimited by a bifurcation on one side and the conjunction of λ_2 and λ_3 local minima on another side.

3.2.1. Bifurcation and reconnection process

To explain the relationship between bifurcations and the emergence of bistability, as observed in Fig. 5(b), we present a sequence of periodic attractors obtained along the interval $\nu \in (0.7, 0.755)$. Fig. 6(a) shows a magnification of the bifurcation diagram in the aforementioned range. Subintervals featuring symmetric-pair of attractors are highlighted in a gray background. Furthermore, each subinterval is numbered and associated with the periodic attractors illustrated in Fig. 6(b).

In the ranges identified by odd numbers in Fig. 6(a), the disturbed Rypdal model presents a single attractor, while in even ones, there is

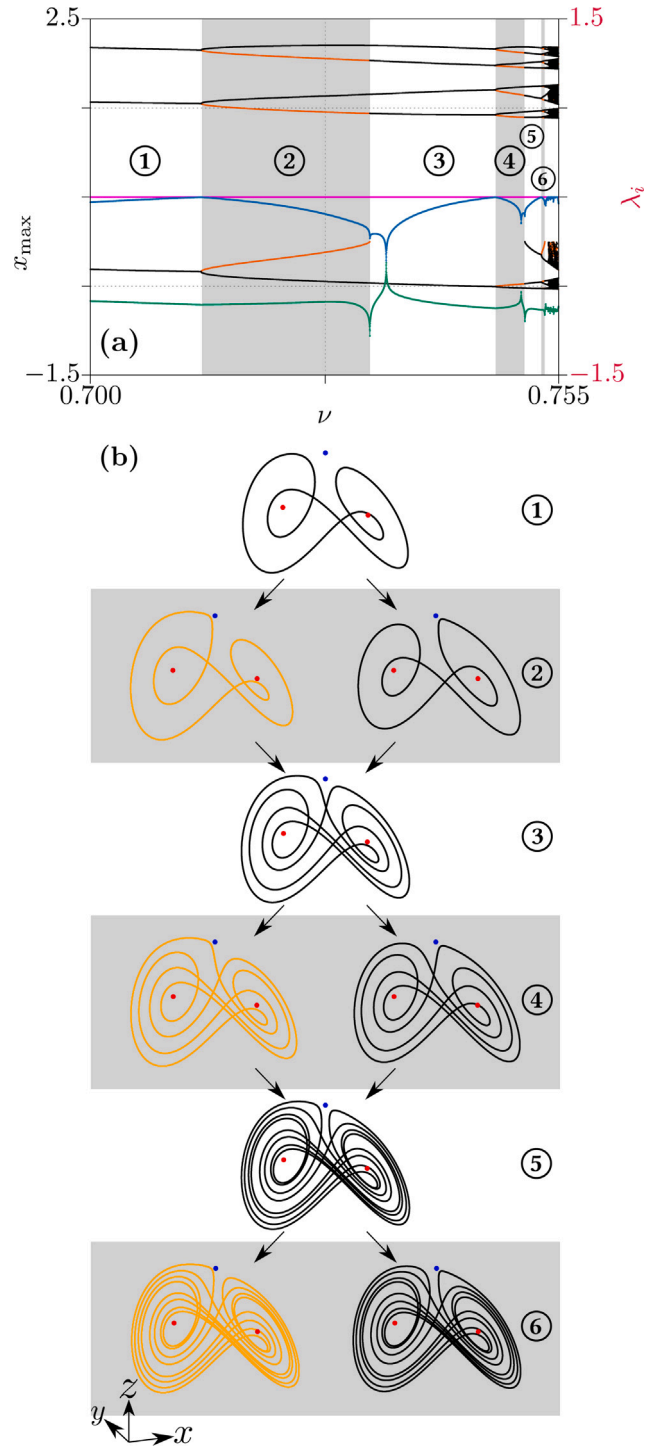


Fig. 6. (a) Magnification of the bifurcation diagram shown in Fig. 5(b), with $\nu \in (0.7, 0.755)$. The subintervals where occur symmetric-pairs of attractors are highlighted in gray background. (b) Sequence of periodic attractors examples found in the corresponding numbered subintervals. From even to odd regions, a collision of the symmetric-pair orbits generates a single attractor. There is I_3 in ① and ② subintervals, I_5 in ③ and ④, and I_{11} in ⑤ and ⑥.

bistability. The first subinterval has a periodic attractor of 3 isospikes. At $\nu \approx 0.713$, the system undergoes a pitchfork bifurcation, delimitating the border between ① and ② subintervals. After the bifurcation, a I_3 symmetric-pair of periodic attractors occurs, until these two collide in the vicinity of the O saddle point at $\nu \approx 0.733$. This collision entails a reconnection and results in a single I_5 periodic attractor in

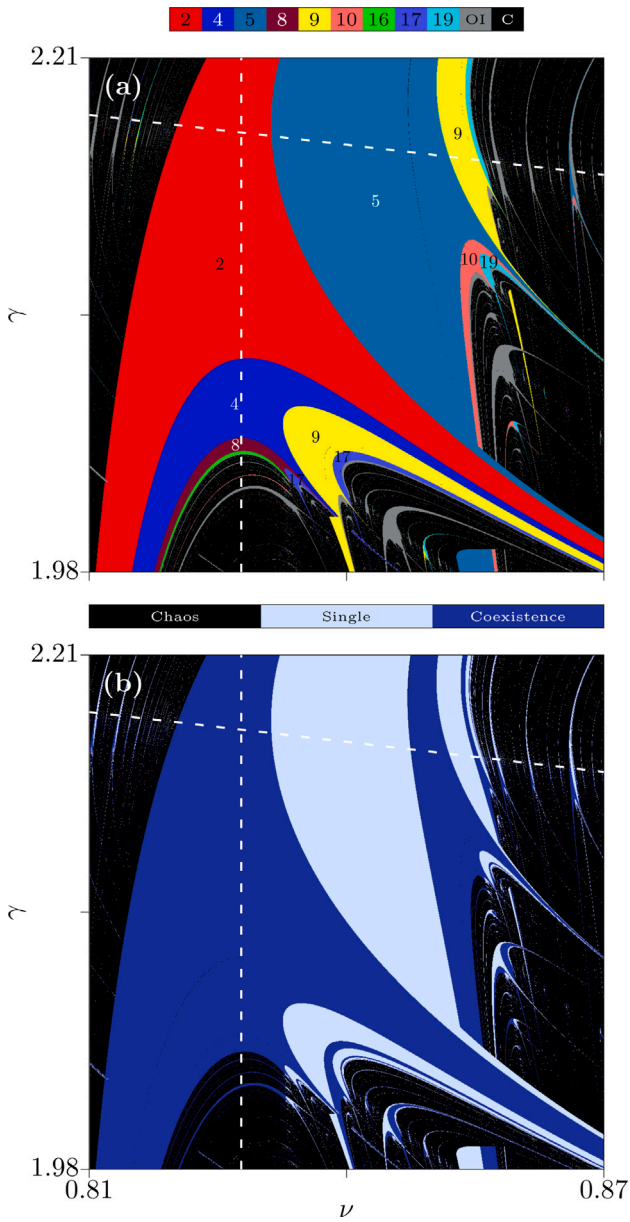


Fig. 7. Magnification of highlighted box in: (a) Fig. 5(a.2) of isospikes for x variable; (b) Fig. 5(a.3) of the periodic attractors coexistence forming symmetric-pairs. Vertical dashed line in $\nu = 0.8278$ and the approximately horizontal is $\gamma(\nu)$ according to Eq. (16).

③. Around $\nu \approx 0.747$, occurs another bifurcation, giving rise to a pair of I_5 periodic attractors coexisting along the range ④, until the reconnection at $\nu \approx 0.751$, leading to a single I_{11} attractor in ⑤. In this way, the cascade of bifurcations and reconnections occurs. Being with a single attractor \mathcal{A} , $T(\mathcal{A}) = \mathcal{A}$ is verified, i.e., the single attractor is symmetric under transformation (2). This internal symmetry is broken at the bifurcation, leading to a symmetric-pair, which reconnects where the local minima of λ_2 and λ_3 are together, meaning greater stability during such reconnection.

Additionally the sequence of periodic attractors generated via bifurcations and reconnections, there are also period-doubling bifurcation cascades. Both routes lead to chaos. Fig. 7 displays magnifications of the highlighted boxes in Figs. 5(a.2–3). Panel Fig. 7(a) shows the isospike diagram for the x variable, complementing panel (b) for the coexistence of periodic attractors in a symmetric-pair. The bistable I_2 region (red) presents a bifurcation to I_4 (blue) in the vertical direction: next I_4 goes to I_8 (brown) and continues in a period-doubling cascade

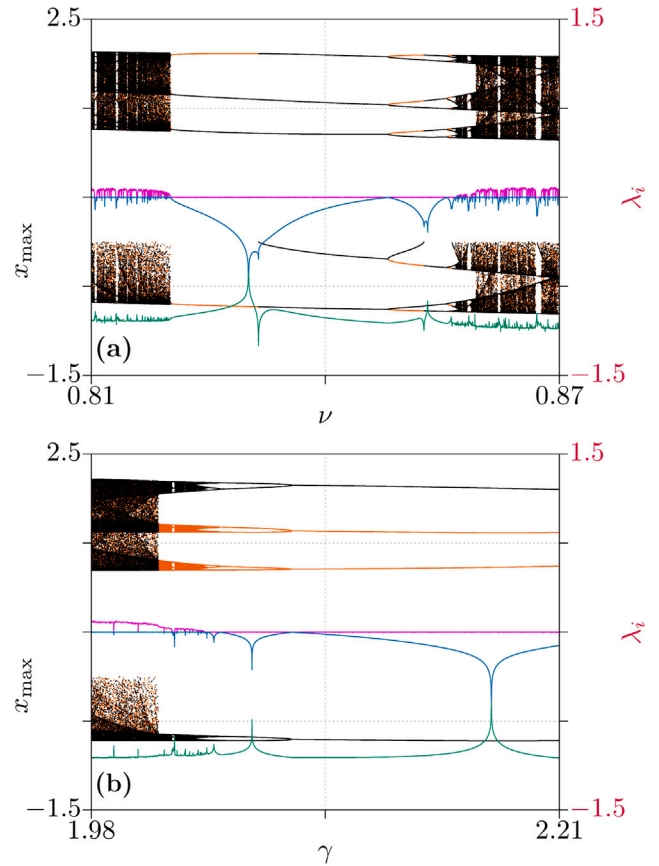


Fig. 8. Local maxima of the x variable and Lyapunov spectrum overlaid. Attractors obtained from the initial conditions $C_0(0.01,0.01,0.01)$ (black dots) and $T(C_0) = C'_0(-0.01,-0.01,0.01)$ (orange dots). Exponents: λ_1 (magenta), λ_2 (blue) and λ_3 (green). Results along the two dashed lines in Figs. 7, being: (a) $\gamma(\mu)$ (approximately horizontal curve); (b) $\nu = 0.8278$ (vertical one). (For interpretation of the references to color in this figure legend, the reader is referred to the web version of this article.)

maintaining bistability. Following the other direction, the same process illustrated in Fig. 6 occurs. The I_2 symmetric-pair reconnects, forming a single I_5 (teal) attractor, which subsequently bifurcates to a pair of I_5 symmetric attractors until their reconnection, resulting in a single I_9 region (yellow). Similarly, from I_4 to I_9 and then to I_{17} (violet color). The bifurcation diagram along $\gamma(\nu)$ shown in Fig. 8(a) corroborates this analysis. Even so, regions resulting from this process present a period-doubling direction, as seen from I_5 to I_{10} (salmon color).

Fig. 8(b) displays a diagram of x variable local maxima and Lyapunov spectrum of orbits along $\nu = 0.8278$ (Figs. 7 vertical dashed line). The period-doubling cascade maintains the bistability, where an attractor (black dots) results from the initial condition C_0 , while another one (orange dots) is from $C'_0 = T(C_0)$. The bifurcation sequence from both initial conditions leads to chaos, where a symmetric-pair of chaotic attractors are found. Near $\gamma \approx 2.02$, a sudden expansion of the chaotic attractors occurs due to an internal crisis [40].

A detailed examination of the attractors structure, focused on the reconnection phenomenon, reveals that the isospikes of the resulting single attractor depend on the collision direction close to the O saddle point. From the reconnection of two I_p periodic attractors of a symmetric-pair, a single orbit I_{2p-1} or I_{2p+1} is obtained, as shown in Fig. 6(b) from I_3 to I_5 and from I_5 to I_{11} . Subsequent reconnections alternate, adding one unit to (or subtracting from) twice the previous isospikes count. Following the sequence of reconnections and pitchfork bifurcations from the shrimp start-band of p_0 isospikes to the adjacent

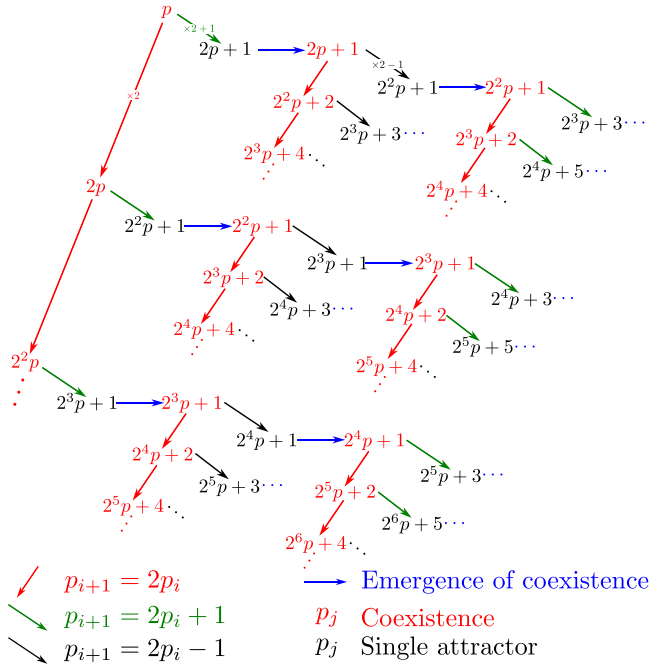


Fig. 9. Schematic representation of the bifurcations and reconnection process within the shrimp-shaped structure. Isospike counts into the period-doubling and bifurcation-reconnection routes to chaos.

region of p_1 , the n th value is given by

$$p_n = \begin{cases} 2^n p_0 + \frac{2^n - (-1)^n}{3}, & \text{if } p_1 = 2p_0 + 1 \\ 2^n p_0 - \frac{2^n - (-1)^n}{3}, & \text{if } p_1 = 2p_0 - 1. \end{cases} \quad (17)$$

Fig. 9 illustrates the isospikes formation rules inside a shrimp, combining period-doubling and the bifurcation-reconnection routes. For simplicity, in this figure, we only use the isospike counts, omitting the letter I . Red arrows represent period-doubling bifurcation, which occurs in bistable regions and takes from I_p to I_{2p} orbits. Blue arrows represent global bifurcations where there are no changes in the isospikes number, but a single I_p attractor bifurcates to a symmetric-pair. The symmetric pair merger scenarios are denoted by: Green arrow if the reconnection of two I_p attractors results in a single I_{2p+1} attractor; black arrow if the reconnection of two I_p attractors leading to a single one with I_{2p-1} . Additionally, period numbers in red indicate symmetric-pair of attractors, while the ones in black represent single attractive orbits.

3.3. Bistability of attractors in a symmetric-pair

Taking into account the coexistence of periodic attractors phenomenon, in this subsection, we investigate bistability in the exponentially disturbed Rypdal model. To this end, we select three parametric configurations in which symmetric-pair of attractors occur. Therefore, we evaluate the attraction basins over two sets of initial conditions: (a) the first one with $z_0 = 0$ and $x_0, y_0 \in (-5, 5]$; (b) the second with $y_0 = -vx_0$ and $x_0, z_0 \in (-5, 5]$. Both planes pass on the N_{\pm} fixed points. Fig. 10(a) is a schematic representation of the first plane (violet color) crossing the I_3 periodic attractors and passing on the two saddle-foci (red dots). Fig. 10(b) illustrates the second plane (cyan), which also crosses the attractors and, in addition to the N_{\pm} , passes on the O saddle point (blue dot).

The adopted values for the parameters concern periodic attractors with different isospike counts in the x variable time series, being indexed as:

1. $(v, \gamma) = (0.730030, 2.2218268)$ with I_3 ;
2. $(v, \gamma) = (0.750050, 2.2133086)$ with I_5 ;
3. $(v, \gamma) = (0.753075, 2.2120188)$ with I_{11} .

These parametric configurations correspond, in this order, to subintervals ②, ④, and ⑥ shown in Fig. 6. By combining the parametric configuration index with those of the initial condition planes, we identify the six panels showing the attraction basins in Figs. 10(a.1–3) and Figs. 10(b.1–3).

The planes of initial conditions were discretized in a uniform grid of 1000×1000 points. For each point on this grid, we numerically evolve the system, and after discarding a transient, the periodic attractors \mathcal{A} and $\mathcal{A}' = T(\mathcal{A})$ are distinguished by the local maxima in the x variable time series. Then, we identify in color the attraction basins \mathcal{B} (black) and \mathcal{B}' (orange), of \mathcal{A} and \mathcal{A}' , respectively.

Figs. 10(a.1–3) emphasize the symmetry between the two basins, where $\mathcal{B}' = T(\mathcal{B})$ with each one covering half of the plane. The same is observed in panels (b.1–3), in which the change $x_0 \mapsto -x_0$ leads from \mathcal{B} to \mathcal{B}' , and vice-versa. A notable aspect is the bands narrowing with rising isospikes, then the structure becomes more intricate as the symmetric-pair's period increases. Due to the basins fractal-like shape, there are initial conditions regions of great uncertainty as the attractor will be obtained from the symmetric-pair, a fact that extends to the entire plane with higher isospike values.

Along the bifurcation and reconnection cascade, a succession of separation and fusion of attraction basins occurs. The bifurcation of a single attractor in a symmetric-pair is related to the initial conditions planes separation into two intricately arranged attraction basins, one for each attractor of the pair. The subsequent reconnection, leading from the symmetric-pair to a single attractor, merges the basins.

4. Conclusions

We propose an exponential parametric disturbance to the Rypdal model, which describes the low-dimensional convection of confined plasmas in the Helimak configuration. The included disturbance results in a third unstable equilibrium point, in addition to the two already present in the undisturbed system. By analyzing the linear stability of these equilibria, we identify a condition for the Andronov–Hopf bifurcation and a region in the parameter space where a saddle-foci pair occurs. We also show two transformations applied to the model, both valid for the systems with and without disturbance. The first transformation is related to the system symmetry, the second is a rescaling, where we reduce one dimension of the parameter space.

Evaluating the disturbed system dynamics in a parameter plane, we identified shrimp spirals immersed in a chaotic region, common in systems satisfying the Shilnikov criterion. Along these periodic structures, bistable bands are alternated with single attractor ones. In the bistability areas, there are a symmetric-pair of attractors, according to the systems symmetry. Into shrimp-shaped domains, two routes to chaos are present, being: (i) a period-doubling cascade, which occurs in the bistable bands; and (ii) a sequence of bifurcation and reconnection processes. In the second route, the bifurcation leads from a single periodic attractor to a symmetric-pair, maintaining the isospike count and giving rise to a bistable region. Subsequently, the pair of attractors collide, resulting in a single attractor band, where the number of isospikes increases. The additional saddle point, due to the exponential perturbation, is essential for this reconnection process. The attractors' collision occurs in the vicinity of this equilibrium, being governed by the corresponding manifolds.

By means of the combined informations about the coexistence of symmetric attractors and isospikes counting, we schematize a new hierarchical organization of periodic attractors within the shrimp-shaped domains, where the isospikes number obeys a combination of two rules.

As a perspective for future development, we will study how the process of symmetric-pair reconnection occurs in terms of the equilibrium points invariant manifolds. With special interest in the role of the saddle point O stable manifold for the merger of attractive orbits in a single attractor.

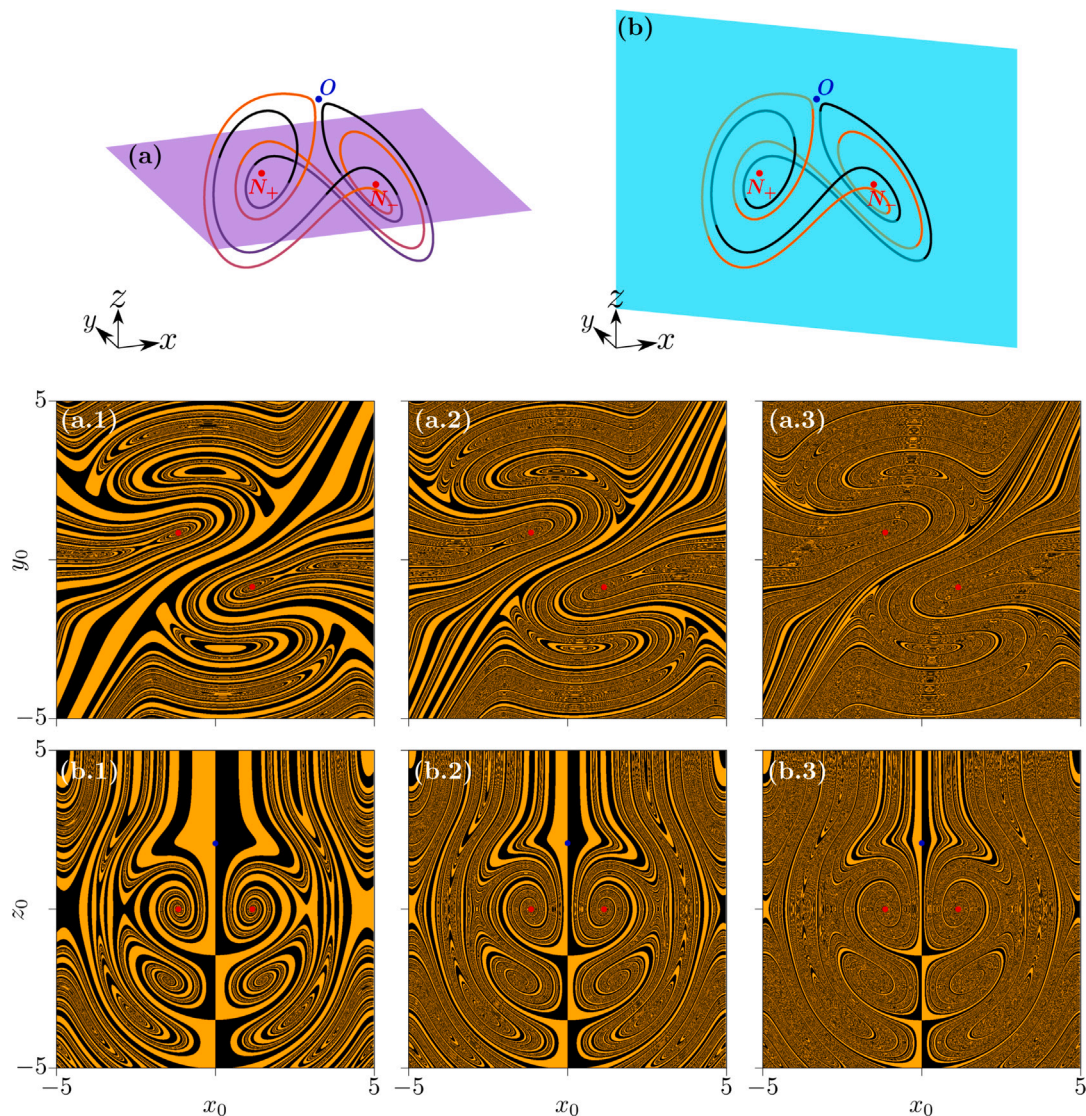


Fig. 10. Schematic representations of the planes (a) $z_0 = 0$ and (b) $y_0 = -vx_0$ crossing the symmetric-pair of periodic attractors. Highlighted the N_{\pm} saddle-foci (red dots) and O saddle points. The six panels with attraction basins \mathcal{B} (black color) and \mathcal{B}' (orange color) are identified according to the aforementioned planes, with parametric configurations in: (a.1) and (b.1) $(\nu, \gamma) = (0.730030, 2.2218268)$ for I_3 attractors; (a.2) and (b.2) $(\nu, \gamma) = (0.750050, 2.2133086)$ for I_3 attractors; (a.3) and (b.3) $(\nu, \gamma) = (0.753075, 2.2120188)$ for I_{11} attractors. (For interpretation of the references to color in this figure legend, the reader is referred to the web version of this article.)

CRediT authorship contribution statement

Arnold A. Alvarez: Writing – review & editing, Writing – original draft, Validation, Software, Methodology, Investigation, Formal analysis, Data curation, Conceptualization. **Eduardo L. Brugnago:** Writing – review & editing, Writing – original draft, Validation, Supervision, Software, Methodology, Investigation, Formal analysis, Data curation, Conceptualization. **I.L. Caldas:** Writing – review & editing, Supervision, Resources, Project administration, Funding acquisition.

Declaration of competing interest

The authors declare that they have no known competing financial interests or personal relationships that could have appeared to influence the work reported in this paper.

Data availability

Data will be made available on request.

Acknowledgments

The authors thank the financial support from the São Paulo Research Foundation (FAPESP, Brazil) under grants #2021/14350-0, #2021/12232-0 and #2018/03211-6; and CNPq #304616/2021-4.

References

- [1] Reis AS, Brugnago EL, Viana RL, Batista AM, Iarosz KC, Ferrari FAS, et al. The role of the fitness model in the suppression of neuronal synchronous behavior with three-stage switching control in clustered networks. *Chaos Solitons Fractals* 2023;167:113122. <http://dx.doi.org/10.1016/j.chaos.2023.113122>.
- [2] Gabrick EC, Brugnago EL, de Souza SLT, Iarosz KC, Szezech Jr JD, Viana RL, et al. Impact of periodic vaccination in SEIRS seasonal model. *Chaos* 2024;34(1):013137. <http://dx.doi.org/10.1063/5.0169834>.
- [3] Brugnago EL, da Silva RM, Manchein C, Beims MW. How relevant is the decision of containment measures against COVID-19 applied ahead of time? *Chaos Solitons Fractals* 2020;140:110164. <http://dx.doi.org/10.1016/j.chaos.2020.110164>.
- [4] da Silva EC, Caldas IL, Viana RL. Bifurcations and onset of chaos on the ergodic magnetic limiter mapping. *Chaos Solitons Fractals* 2002;14(3):403–23. [http://dx.doi.org/10.1016/S0960-0779\(01\)00133-3](http://dx.doi.org/10.1016/S0960-0779(01)00133-3).

- [5] Lorenz EN. Deterministic nonperiodic flow. *J Atmos Sci* 1963;20(2):130–41. [http://dx.doi.org/10.1175/1520-0469\(1963\)020<0130:DNF>2.0.CO;2](http://dx.doi.org/10.1175/1520-0469(1963)020<0130:DNF>2.0.CO;2).
- [6] Rössler OE. An equation for continuous chaos. *Phys Lett A* 1976;57(5):397–8. [http://dx.doi.org/10.1016/0375-9601\(76\)90101-8](http://dx.doi.org/10.1016/0375-9601(76)90101-8).
- [7] Rikitake T. Oscillations of a system of disk dynamos. In: *Math. proc. camb. philos. soc.*, vol. 54, (no. 1):Cambridge University Press; 1958, p. 89–105. <http://dx.doi.org/10.1017/S0305004100033223>.
- [8] Chua LO, Komuro M, Matsumoto T. The double scroll family. *IEEE Trans Circuits Syst* 1986;33(11):1072–118. <http://dx.doi.org/10.1109/TCS.1986.1085869>.
- [9] Mathias AC, Rech PC. Changes in the dynamics of a Rössler oscillator by an external forcing. *Chin Phys Lett* 2013;30(3):030502. <http://dx.doi.org/10.1088/0256-307X/30/3/030502>.
- [10] Rech PC. How to embed shrimps in parameter planes of the Lorenz system. *Phys Scr* 2017;92(4):045201. <http://dx.doi.org/10.1088/1402-4896/aa5f61>.
- [11] Correia MJ, Rech PC. Hyperchaotic states in the parameter-space. *Appl Math Comput* 2012;218(12):6711–5. <http://dx.doi.org/10.1016/j.amc.2011.12.035>.
- [12] Medeiros ES, de Souza SLT, Medrano-T RO, Caldas IL. Replicate periodic windows in the parameter space of driven oscillators. *Chaos Solitons Fractals* 2011;44(11):982–9. <http://dx.doi.org/10.1016/j.chaos.2011.08.002>.
- [13] de Souza SLT, Lima AA, Caldas IL, Medrano-T. RO, Guimarães-Filho ZO. Self-similarities of periodic structures for a discrete model of a two-gene system. *Phys Lett A* 2012;376(15):1290–4. <http://dx.doi.org/10.1016/j.physleta.2012.02.036>.
- [14] Lorenz EN. Compound windows of the Hénon-map. *Phys D* 2008;237(13):1689–704. <http://dx.doi.org/10.1016/j.physd.2007.11.014>.
- [15] Gallas JAC. Structure of the parameter space of the Hénon map. *Phys Rev Lett* 1993;70:2714–7. <http://dx.doi.org/10.1103/PhysRevLett.70.2714>.
- [16] Gallas JAC. Stability diagrams for a memristor oscillator. *Eur Phys J : Spec Top* 2019;228:2081–91. <http://dx.doi.org/10.1140/epjst/e2019-900009-8>.
- [17] Gallas JAC. Chapter three - spiking systematics in some CO2 laser models. In: Arimondo E, Lin CC, Yelin SF, editors. In: *Advances in atomic, molecular, and optical physics*, vol. 65, Academic Press; 2016, p. 127–91. <http://dx.doi.org/10.1016/bs.aamop.2016.01.001>.
- [18] Barrio R, Blesa F, Serrano S, Shilnikov A. Global organization of spiral structures in biparameter space of dissipative systems with shilnikov saddle-foci. *Phys Rev E* 2011;84:035201. <http://dx.doi.org/10.1103/PhysRevE.84.035201>.
- [19] Albuquerque HA, Rubinger RM, Rech PC. Self-similar structures in a 2D parameter-space of an inductorless Chua's circuit. *Phys Lett A* 2008;372(27):4793–8. <http://dx.doi.org/10.1016/j.physleta.2008.05.036>.
- [20] Malykh S, Bakhanova Y, Kazakov A, Pusuluri K, Shilnikov AL. Homoclinic chaos in the Rössler model. *Chaos* 2020;30(11):113126. <http://dx.doi.org/10.1063/5.0026188>.
- [21] Medrano-T. RO, Caldas IL. Periodic windows distribution resulting from homoclinic bifurcations in the two-parameter space. 2010, [arXiv:1012.2241](https://arxiv.org/abs/1012.2241).
- [22] Stoop R, Benner P, Uwate Y. Real-world existence and origins of the spiral organization of shrimp-shaped domains. *Phys Rev Lett* 2010;105:074102. <http://dx.doi.org/10.1103/PhysRevLett.105.074102>.
- [23] Bykov VV. The bifurcations of separatrix contours and chaos. *Phys D* 1993;62(1):290–9. [http://dx.doi.org/10.1016/0167-2789\(93\)90288-C](http://dx.doi.org/10.1016/0167-2789(93)90288-C).
- [24] Glendinning P, Sparrow C. Local and global behavior near homoclinic orbits. *J Stat Phys* 1984;35:645–96. <http://dx.doi.org/10.1007/BF01010828>.
- [25] Shilnikov LP, Shilnikov AL, Turaev DV, Chua LO. *Methods of qualitative theory in nonlinear dynamics*. World Scientific; 2001, <http://dx.doi.org/10.1142/4221>.
- [26] Wei Z, Yang Q. Controlling the diffusionless Lorenz equations with periodic parametric perturbation. *Comput Math Appl* 2009;58(10):1979–87. <http://dx.doi.org/10.1016/j.camwa.2009.07.058>.
- [27] Wang Z, Xi X, Sun W. Stabilizing DLEs system with periodic parametric perturbations using backstepping control. In: *2013 IEEE third international conference on information science and technology*. 2013, p. 102–5. <http://dx.doi.org/10.1109/ICIST.2013.6747509>.
- [28] Rypdal K, Garcia OE. In: *Profile robustness and routes to turbulence in the helimak configuration*, vol. 29C, 2005, p. P–2. 034, URL http://ocs.ciemat.es/EPS2005/pdf/P2_034.pdf. 32nd European Physical Society Conference on Plasma Physics.
- [29] Rypdal K, Živkovic T. Low-dimensional convection dynamics in the helimak configuration. In: *35th EPS conference on plasma physics 2008, EPS 2008 - europhysics conference abstracts*. 2008.
- [30] Bonatto C, Gallas JAC. Periodicity hub and nested spirals in the phase diagram of a simple resistive circuit. *Phys Rev Lett* 2008;101(5):054101. <http://dx.doi.org/10.1103/PhysRevLett.101.054101>.
- [31] Letellier C, Gilmore R. Covering dynamical systems: Twofold covers. *Phys Rev E* 2000;63:016206. <http://dx.doi.org/10.1103/PhysRevE.63.016206>.
- [32] Fehlberg E. Klassische Runge-Kutta-Formeln fünfter und siebenter Ordnung mit Schrittwelten-Kontrolle. *Computing* 1969;4:93–106. <http://dx.doi.org/10.1007/BF02234758>.
- [33] Sprott JC. Some simple chaotic flows. *Phys Rev E* 1994;50:647–50. <http://dx.doi.org/10.1103/PhysRevE.50.R647>.
- [34] Letellier C, Mendes EMAM, Malasoma J-M. Lorenz-like systems and Lorenz-like attractors: Definition, examples, and equivalences. *Phys Rev E* 2023;108:044209. <http://dx.doi.org/10.1103/PhysRevE.108.044209>.
- [35] Byrne G, Gilmore R, Letellier C. Distinguishing between folding and tearing mechanisms in strange attractors. *Phys Rev E* 2004;70:056214. <http://dx.doi.org/10.1103/PhysRevE.70.056214>.
- [36] Wolf A, Swift JB, Swinney HL, Vastano JA. Determining Lyapunov exponents from a time series. *Phys D* 1985;16(3):285–317. [http://dx.doi.org/10.1016/0167-2789\(85\)90011-9](http://dx.doi.org/10.1016/0167-2789(85)90011-9).
- [37] Benettin G, Galgani L, Giorgilli A, Strelcyn J. Lyapunov characteristic exponents for smooth dynamical systems and for Hamiltonian systems; A method for computing all of them. Part 1: Theory. *Meccanica* 1980;15:9–20. <http://dx.doi.org/10.1007/BF02128236>.
- [38] Prince PJ, Dormand JR. High order embedded Runge-Kutta formulae. *J Comput Appl Math* 1981;7(1):67–75. [http://dx.doi.org/10.1016/0771-050X\(81\)90010-3](http://dx.doi.org/10.1016/0771-050X(81)90010-3).
- [39] van der Schrier G, Maas LRM. The diffusionless Lorenz equations; Shil'nikov bifurcations and reduction to an explicit map. *Phys D* 2000;141(1):19–36. [http://dx.doi.org/10.1016/S0167-2789\(00\)00033-6](http://dx.doi.org/10.1016/S0167-2789(00)00033-6).
- [40] Grebogi C, Ott E, Yorke JA. Crises, sudden changes in chaotic attractors, and transient chaos. *Phys D* 1983;7(1):181–200. [http://dx.doi.org/10.1016/0167-2789\(83\)90126-4](http://dx.doi.org/10.1016/0167-2789(83)90126-4).
- [41] Meinsma G. Elementary proof of the Routh-Hurwitz test. *Systems Control Lett* 1995;25(4):237–42. [http://dx.doi.org/10.1016/0167-6911\(94\)00089-E](http://dx.doi.org/10.1016/0167-6911(94)00089-E).
- [42] Kuznetsov YA. *Elements of applied bifurcation theory*. In: *Applied mathematical sciences*, Springer New York; 2004, <http://dx.doi.org/10.1007/978-1-4757-3978-7>.
- [43] Gallas JAC. Overlapping adding-doubling spikes cascades in a semiconductor laser proxy. *Braz J Phys* 2021;51(4):919–26. <http://dx.doi.org/10.1007/s13538-021-00865-z>.